Broadband and Resonant Approaches to Axion Dark Matter Detection

Yonatan Kahn,[1,*] Benjamin R. Safdi,[2,†] and Jesse Thaler[2,‡]

[1]*Department of Physics, Princeton University, Princeton, New Jersey 08544, USA*
[2]*Center for Theoretical Physics, Massachusetts Institute of Technology, Cambridge, Massachusetts 02139, USA*

When ultralight axion dark matter encounters a static magnetic field, it sources an effective electric current that follows the magnetic field lines and oscillates at the axion Compton frequency. We propose a new experiment to detect this axion effective current. In the presence of axion dark matter, a large toroidal magnet will act like an oscillating current ring, whose induced magnetic flux can be measured by an external pickup loop inductively coupled to a SQUID magnetometer. We consider both resonant and broadband readout circuits and show that a broadband approach has advantages at small axion masses. We estimate the reach of this design, taking into account the irreducible sources of noise, and demonstrate potential sensitivity to axionlike dark matter with masses in the range of 10^{-14}-10^{-6} eV. In particular, both the broadband and resonant strategies can probe the QCD axion with a GUT-scale decay constant.

A broad class of well-motivated dark matter (DM) models consists of light pseudoscalar particles a coupled weakly to electromagnetism [1–3]. The most famous example is the QCD axion [4–7], which was originally proposed to solve the strong CP problem. More generally, string compactifications often predict a large number of axionlike particles (ALPs) [8], with Planck-suppressed couplings to electric ($\mathbf{E}$) and magnetic ($\mathbf{B}$) fields of the form $a\mathbf{E} \cdot \mathbf{B}$. Unlike QCD axions, generic ALPs do not necessarily couple to the QCD operator $G\tilde{G}$, where G is the QCD field strength. The masses and couplings of ALP DM candidates are relatively unconstrained by theory or experiment (see Refs. [9–11] for reviews). It is therefore important to develop search strategies that cover many orders of magnitude in the axion parameter space.

The ADMX experiment [12–14] has already placed stringent constraints on axion DM in a narrow mass range around $m_a \sim$ few $\times 10^{-6}$ eV. However, ADMX is only sensitive to axion DM whose Compton wavelength is comparable to the size of the resonant cavity. For the QCD axion, the axion mass m_a is related to the Peccei-Quinn (PQ) symmetry-breaking scale f_a via

$$f_a m_a \simeq f_\pi m_\pi, \qquad (1)$$

where $m_\pi \approx 140$ MeV ($f_\pi \approx 92$ MeV) is the pion mass (decay constant). Lighter QCD axion masses therefore correspond to higher-scale axion decay constants f_a. The GUT scale ($f_a \sim 10^{16}$ GeV, $m_a \sim 10^{-9}$ eV) is particularly well motivated, but well beyond the reach of ADMX as such small m_a would require much larger cavities. More general ALPs can also have lighter masses and larger couplings than in the QCD case.

In this Letter, we propose a new experimental design for axion DM detection that targets the mass range $m_a \in [10^{-14}, 10^{-6}]$ eV. Like ADMX, this design exploits the fact that axion DM, in the presence of a static magnetic field, produces response electromagnetic fields that oscillate at the axion Compton frequency. Whereas ADMX is based on resonant detection of a cavity excitation, our design is based on either broadband or resonant detection of an oscillating magnetic flux with sensitive magnetometers, sourced by an axion effective current. Our static magnetic field is generated by a superconducting toroid, which has the advantage that the flux readout system can be external to the toroid, in a region of ideally zero static field. Crucially, this setup can probe axions whose Compton wavelength is much larger than the size of the toroid. If this experiment were built, we propose the acronym ABRACADABRA, for "A Broadband or Resonant Approach to Cosmic Axion Detection with an Amplifying B-field Ring Apparatus."

For ultralight (sub-eV) axion DM, it is appropriate to treat a as a coherent classical field, since large DM number densities imply macroscopic occupation numbers for each quantum state. Solving the classical equation of motion with zero DM velocity yields

$$a(t) = a_0 \sin(m_a t) = \frac{\sqrt{2\rho_{\mathrm{DM}}}}{m_a} \sin(m_a t), \qquad (2)$$

where $\rho_{\mathrm{DM}} \approx 0.3$ GeV/cm^3 is the local DM density [15]. (The local virial DM velocity $v \sim 10^{-3}$ will give small spatial gradients $\nabla a \propto v$.) Through the coupling to the QED field strength $F_{\mu\nu}$,

$$\mathcal{L} \supset -\frac{1}{4} g_{a\gamma\gamma} a F_{\mu\nu} \tilde{F}^{\mu\nu}, \qquad (3)$$

a generic axion will modify Maxwell's equations [16], and Ampère's circuit law becomes

$$\nabla \times \mathbf{B} = \frac{\partial \mathbf{E}}{\partial t} - g_{a\gamma\gamma} \left(\mathbf{E} \times \nabla a - \mathbf{B} \frac{\partial a}{\partial t} \right), \qquad (4)$$

with similar modifications to Gauss's law. For the QCD axion, $g_{a\gamma\gamma} = g\alpha_{EM}/(2\pi f_a)$, where α_{EM} is the electromagnetic fine-structure constant and g is an $\mathcal{O}(1)$ number equal to ~ 0.75 (-1.92) for the DFSZ model [17,18] (KSVZ model [19,20]). Thus, in the presence of a static magnetic background $\mathbf{B}_0$, there is an axion-sourced effective current

$$\mathbf{J}_{eff} = g_{a\gamma\gamma}\sqrt{2\rho_{DM}}\cos(m_a t)\mathbf{B}_0. \qquad (5)$$

This effective current then sources a real magnetic field, oscillating at frequency m_a, that is perpendicular to $\mathbf{B}_0$.

Our proposed design is shown schematically in Fig. 1. The static magnetic field $\mathbf{B}_0$ is generated by a constant current in a superconducting wire wrapping a toroid, and the axion effective current is detected with a superconducting pickup loop in the toroid hole. In the absence of axion DM (or noise), there is no magnetic flux through the pickup loop. With axion DM, there will be an oscillating magnetic flux through the pickup loop proportional to $\sqrt{\rho_{DM}}$. This design is inspired by cryogenic current comparators (CCCs) [21], which are used for measuring real currents. The key difference here is the static external field $\mathbf{B}_0$, which generates an effective electric current in the presence of axion DM instead of the real current in the case of the CCC.

In a real implementation of both designs, the signal flux is actually sourced by a Meissner current which returns along the outside surface of a gapped toroid. The size of the gap is not crucial for our analysis, but must be sufficiently large that parasitic capacitance effects do not generate a displacement current, which might shunt the Meissner return current and reduce the induced signal B field. For wires of diameter 1 mm and a meter-sized toroid, a gap of a few millimeters allows unscreened currents up to the frequency at which the magnetoquasistatic approximation breaks down and displacement currents are unavoidable. In what follows, we will estimate our sensitivity using the axion effective current which is correct up to $\mathcal{O}(1)$ geometric factors.
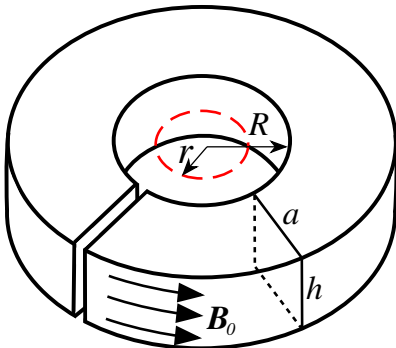

FIG. 1. A (gapped) toroidal geometry to generate a static magnetic field $\mathbf{B}_0$. The dashed red circle shows the location of the superconducting pickup loop of radius $r \leq R$. The gap ensures a return path for the Meissner screening current; see discussion in main text.

We consider two distinct circuits for reading out the signal, both based on a superconducting quantum interference device (SQUID). The broadband circuit uses a untuned magnetometer in an ideally zero-resistance setup, while the resonant circuit uses a tuned magnetometer with irreducible resistance. Both readout circuits can probe multiple orders of magnitude in the axion DM parameter space, though the broadband approach has increased sensitivity at low axion masses.

A related proposal, utilizing the axion effective current, was put forth recently by Ref. [22] (see also Ref. [23] for a preliminary proposal and Ref. [24] for a similar design for detecting dark photon DM). That design was based on a solenoidal magnetic field, with the pickup loop located inside of the solenoid, and focused on resonant readout using an LC circuit. The design presented here offers a few advantages. First, the toroidal geometry significantly reduces fringe fields compared to a solenoidal geometry. Second, the pickup loop is located in an ideally zero-field region, outside of the toroidal magnetic field $\mathbf{B}_0$, which should help reduce flux noise. Third, as we will show, broadband readout has significant advantages over resonant readout at low axion masses. Our proposal is complementary to the recently proposed CASPEr experiment [25], which probes a similar range of axion masses but measures the coupling to nuclear electric dipole moments rather than the coupling to QED. See Refs. [26–40] for other proposals to detect axion DM.

For concreteness, our sensitivity studies are based on a toroid of rectangular cross section (height h, width a) and inner radius R, as illustrated in Fig. 1. The magnetic field inside the toroid volume is

$$\mathbf{B}_0(s) = B_{max}\frac{R}{s}\hat{\boldsymbol{\phi}}, \qquad (6)$$

where s is the distance from the central axis of the toroid, $\hat{\boldsymbol{\phi}}$ is the azimuthal direction, and B_{max} is the magnitude of $\mathbf{B}_0$ at the inner radius. The flux through the pickup loop of radius $r \leq R$ can be written as

$$\Phi_{pickup}(t) = g_{a\gamma\gamma}B_{max}\sqrt{2\rho_{DM}}\cos(m_a t)V_B. \qquad (7)$$

The effective volume containing the external $\mathbf{B}$ field is

$$V_B = \int_0^r dr' \int_R^{R+a} ds \int_0^{2\pi} d\theta \frac{Rhr'(s - r'\cos\theta)}{\tilde{r}^2\sqrt{h^2 + 4\tilde{r}^2}}, \qquad (8)$$

with $\tilde{r}^2 \equiv s^2 + r'^2 - 2sr'\cos\theta$. We work in the magnetoquasistatic limit, $2\pi/m_a \gg r, R, h, a$; at higher frequencies, displacement currents can potentially screen our signal. As an illustration, we consider a meter-sized experiment, where $V_B = 1$ m^3 for $r = R = a = h/3 = 0.85$ m, with sensitivity to $m_a \lesssim 10^{-6}$ eV. For an example of the magnitude of the generated fields, the average B field sourced by a GUT-scale KSVZ axion ($f_a = 10^{16}$ GeV) with $V_B = 100$ m^3 and $B_{max} = 5$ T is 2.5×10^{-23} T. To
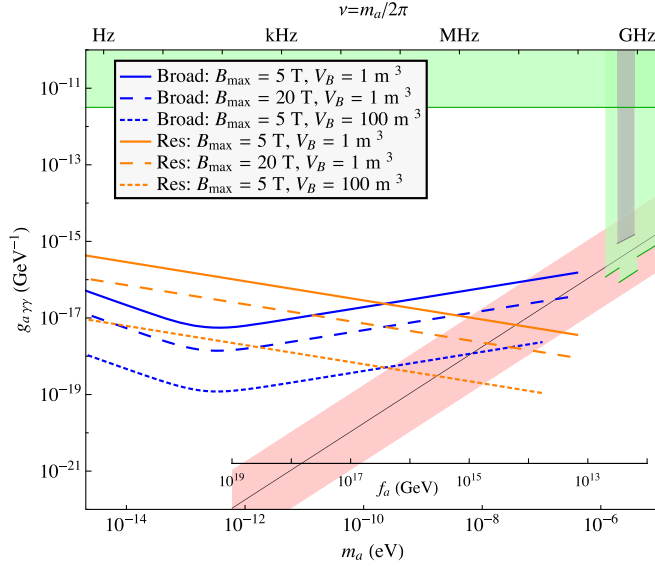
FIG. 2. Anticipated reach in the $g_{a\gamma\gamma}$ vs m_a plane for the broadband (Broad) and resonant (Res) strategies. The benchmark parameters are $T = 0.1$ K, $r = a = R = h/3$ (see Fig. 1), and $L_p = L_{\min} \approx \pi R^2/h$. The total measurement time for both strategies is $t = 1$ yr, where the resonant experiment scans from 1 Hz to 100 MHz. The expected parameters for the QCD axion are shown in shaded red, with the corresponding decay constant f_a inset at bottom right. The projected sensitivities of IAXO [41] and ADMX [14] are shown shaded in light green. Published limits from ADMX [13] are shown in gray.

detect such a small B field at this frequency, we need a flux noise sensitivity of 1.2×10^{-19} Wb/$\sqrt{\text{Hz}}$ for a measurement time of 1 year in a broadband strategy (see below). The anticipated reach for various V_B and $B_{\max}$ is summarized in Fig. 2.

Broadband approach.—In an untuned magnetometer, a change in flux through the superconducting pickup loop induces a supercurrent in the loop. As shown in Fig. 3 (left), the pickup loop (inductance L_p) is connected in series with an input coil L_i, which is inductively coupled to the SQUID (inductance L) with mutual inductance M. The flux through the SQUID is proportional to the flux through the pickup loop and is maximized when $L_i \approx L_p$ [42]:
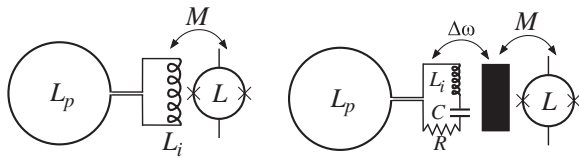

FIG. 3. Schematics of our readout circuits. Left: broadband (untuned magnetometer). The pickup loop L_p is placed in the toroid hole as in Fig. 1 and connected in series with an input coil L_i, which has mutual inductance M with the SQUID of self-inductance L. Right: resonant (tuned magnetometer). L_p is now in series with both L_i and a tunable capacitor C. A "black box" feedback circuit modulates the bandwidth $\Delta\omega$ and has mutual inductance M with the SQUID.

$$\Phi_{\text{SQUID}} \approx \frac{\alpha}{2}\sqrt{\frac{L}{L_p}}\Phi_{\text{pickup}}. \tag{9}$$

Here, α is an $\mathcal{O}(1)$ number, with $\alpha^2 \approx 0.5$ in typical SQUID geometries [43].

Clearly, the flux through the SQUID will be maximized for L as large as possible and L_p as small as possible. A typical SQUID has inductance $L = 1$ nH. A superconducting pickup loop of wire radius $\phi = 1$ mm and loop radius $r = 0.85$ m has geometric inductance of [44]

$$L_p = r(\ln(8r/\phi) - 2) \approx 7 \ \mu\text{H}, \tag{10}$$

but this may be reduced with smaller loops in parallel as in a fractional-turn magnetometer [45,46]. The minimum inductance is limited by the magnetic field energy $(1/2)\int \mathbf{B}^2 dV$ stored in the axion-sourced response field, and is approximately

$$L_{\min} \approx \pi R^2/h. \tag{11}$$

With a "tall" toroid where $h = 3R$, one can achieve $L_{\min} \approx 1 \ \mu\text{H}$ and $\Phi_{\text{SQUID}} \approx 0.01\Phi_{\text{pickup}}$ for $R = 0.85$ m. Since the pickup loop area is much larger than the magnetometer area, the B field felt by the SQUID is significantly enhanced compared to the axion-induced field in the pickup loop. The B-field enhancement takes advantage of the fact that we are working in the near-field limit, so that the induced B field adds coherently over the pickup loop.

To assess the sensitivity of the untuned magnetometer to the axion-sourced oscillating flux in Eq. (7), we must characterize the noise of the circuit. In a pure superconducting circuit at low frequencies, there is zero noise in the pickup loop and input coil, and the only source of noise is in the SQUID, with contributions from thermal fluctuations of both voltage and current. Despite their thermal origin, we will refer to these as "magnetometer noise" to distinguish them from noise in the pickup loop circuit (which dominates in the resonant case below). At cryogenic temperatures ($T \lesssim 60$ mK), thermal current and voltage noise are subdominant to the current shot noise $S_{J,0}$ in the SQUID tunnel junctions [43], which sets an absolute (temperature-independent) floor for the magnetometer noise. See the Supplemental Material [47] for a more detailed discussion of noise in a real implementation of this design.

A typical, temperature-independent flux noise for commercial SQUIDs at frequencies greater than ~ 10 Hz is

$$S_{\Phi,0}^{1/2} \sim 10^{-6}\Phi_0/\sqrt{\text{Hz}}, \tag{12}$$

where $\Phi_0 = h/(2e) = 2.1 \times 10^{-15}$ Wb is the flux quantum. We use this noise level and a fiducial temperature of 0.1 K as our benchmark. dc SQUIDS are also known to exhibit $1/f$ noise, which dominates below about 50 Hz at 0.1 K [48]. We estimate the reach of our broadband strategy down to 1 Hz assuming $1/f$ noise is the sole irreducible source of noise at these low frequencies, but in a realistic

experiment, environmental noise would likely contribute as well; see the Supplemental Material [47] for more details.

Following Ref. [25], the signal-to-noise ratio S/N improves with integration time t as

$$S/N \sim |\Phi_{\text{SQUID}}|(t\tau)^{1/4}/S_{\Phi,0}^{1/2} \qquad (13)$$

for $t > \tau$, where τ is the axion coherence time (when $t < \tau$, $S/N \sim |\Phi_{\text{SQUID}}|\sqrt{t}/S_{\Phi,0}^{1/2}$). The axion coherence time is approximately

$$\tau \sim \frac{2\pi}{m_a v^2} \sim 10^6 \frac{2\pi}{m_a} \approx 3 \times 10^4 \text{s} \left(\frac{10^{-12} \text{ eV}}{m_a}\right), \quad (14)$$

where we have taken $v \sim 10^{-3}$ as the local DM virial velocity. We assume a fiducial integration time of $t = 1$ year, so that $t \gg \tau$ over most of the mass range of interest. We also assume a geometry with $r = R = a = h/3$ and a pickup loop inductance $L_p = L_{\min}$. Then, requiring $S/N > 1$ after time t implies sensitivity to

$$g_{a\gamma\gamma} > 6.3 \times 10^{-18} \text{ GeV}^{-1} \left(\frac{m_a}{10^{-12} \text{ eV}} \frac{1 \text{ year}}{t}\right)^{1/4} \frac{5\text{T}}{B_{\max}}$$

$$\times \left(\frac{0.85 \text{ m}}{R}\right)^{5/2} \sqrt{\frac{0.3 \text{ GeV/cm}^3}{\rho_{\text{DM}}}} \frac{S_{\Phi,0}^{1/2}}{10^{-6}\Phi_0/\sqrt{\text{Hz}}}. \qquad (15)$$

As shown in Fig. 2, an ideal broadband setup with the benchmark parameters in Eq. (15) could begin to probe the QCD axion band for $f_a \lesssim 10^{14}$ GeV, which is not far below the GUT scale. The sensitivity improves for larger magnetic fields or larger toroids; for a toroid with $V_B = 100 \text{ m}^3$, one can probe the QCD axion band at the GUT scale. However, larger experiments may not be sensitive to axion masses near 10^{-6} eV because displacement currents may partially cancel the axion-sourced flux. Note that the sensitivity to $g_{a\gamma\gamma}$ increases at *smaller* m_a, due to the increase in axion coherence time.

Resonant approach.—We now turn to an analysis of a tuned magnetometer, shown in Fig. 3 (right). This readout circuit has the advantage of enhancing the signal by the quality factor Q at the resonant frequency. The tuned circuit is a standard design for detecting small magnetic fields at a given frequency (see, e.g., Ref. [43]). Similar tuned circuits have been considered before for axion DM detection [22] and dark-photon DM detection [24]; our analysis follows closely those of Refs. [24] and [42].

In a practical implementation of an LC circuit with resonant frequency $\omega = 1/\sqrt{LC}$, the capacitor has nonzero intrinsic resistance R. Therefore, the circuit has a finite bandwidth $\Delta\omega_{LC} = \omega/Q_0$, where $Q_0 = (\omega C R)^{-1}$. To maximize the axion signal given the expected bandwidth $\Delta\omega/\omega \simeq 10^{-6}$, the intrinsic bandwidth of the resonant circuit should be set to $\Delta\omega_{LC} = \max[\Delta\omega, 2\pi/\Delta t]$, where Δt is the interrogation time at this frequency. While $Q_0 \simeq 10^6$ is optimal for sufficiently large ω, smaller Q

values are needed at smaller ω to make sure the bandwidth matches the interrogation time. For example, in the strategy of Ref. [24], where each e-fold of frequency is scanned for a time period $t_{e\text{-fold}}$, and thus $\Delta t = t_{e\text{-fold}}/Q_0$, one must take $Q_0 = \min[10^6, \sqrt{\omega t_{e\text{-fold}}/2\pi}]$. Decreasing Q_0, however, means adding additional resistance to the circuit and thereby increasing the thermal noise.

Alternatively, we can employ the feedback damping circuit of Refs. [49,50], which can widen the intrinsic bandwidth of the resonant circuit without introducing additional noise. This allows a large Q factor at all frequencies while still capturing all of the signal [42]. The intrinsic Q_0 of a niobium superconducting LC circuit is over 10^6, so we assume $Q_0 = 10^6$ as our benchmark, though larger Q_0 may be possible. The signal flux through the SQUID depends sensitively on the details of the feedback circuit, but our signal-to-noise analysis will not depend on those details, so we treat the feedback circuit as a black box with some inductive coupling M to the SQUID in Fig. 3 (right).

For Q_0 up to $\sim 10^8$, thermal noise in the pickup loop dominates over magnetometer noise (see related studies in Refs. [24,51] and further discussion in the Supplemental Material [47]). Once we know that thermal noise is dominant, we can calculate the signal-to-noise ratio without regard to the identity of the black box. Following Ref. [24], the axion sensitivity is set by requiring the signal power dissipated in the resonant circuit to be greater than that of the noise. The predicted constraints on $g_{a\gamma\gamma}$ depend on how much time is spent on each frequency band. We imagine a strategy similar to Ref. [24] where each e-fold of frequency is scanned for a time period $t_{e\text{-fold}}$. To compare with the broadband circuit, we take $t_{e\text{-fold}} = 20$ days to cover the frequency range between 1 Hz ($m_a = 4 \times 10^{-15}$ eV) and 100 MHz ($m_a = 4 \times 10^{-7}$ eV) in the same integration time of 1 year.

At frequency m_a, the signal and noise powers are

$$P_S = Q_0 \frac{m_a \Phi_{\text{pickup}}^2}{2L_T}, \qquad P_N = k_B T \sqrt{\frac{m_a}{2\pi t_{e\text{-fold}}}}, \qquad (16)$$

where $L_T = L_p + L_i$ is the total inductance of the resonant circuit. To compare with the broadband reach we assume $L_T = L_{\min}$ as in Eq. (11) and take $h = 3R$. Requiring a signal-to-noise ratio of unity implies sensitivity to

$$g_{a\gamma\gamma} > 9.0 \times 10^{-17} \text{ GeV}^{-1} \left(\frac{10^{-12} \text{ eV}}{m_a} \frac{20 \text{ days}}{t_{e\text{-fold}}}\right)^{1/4}$$

$$\times \frac{5\text{T}}{B_{\max}} \left(\frac{0.85 \text{ m}}{R}\right)^{5/2} \sqrt{\frac{0.3 \text{ GeV/cm}^3}{\rho_{\text{DM}}} \frac{10^6}{Q_0} \frac{T}{0.1 \text{ K}}}, \qquad (17)$$

where we have assumed a feedback damping circuit that allows us to keep Q_0 fixed at low masses. At high masses, the feedback damping circuit is not necessary unless $Q_0 > 10^6$ is achievable.

As illustrated in Fig. 2, the sensitivity increases at *larger* m_a since the signal power density grows as m_a. On the other hand, at small masses the broadband approach has a superior projected reach for the same experimental parameters. Thus, the resonant and broadband approaches are complementary.

We introduced a new experimental design that is sensitive to ultralight DM with axionlike couplings to electromagnetism in the mass range $m_a \in [10^{-14}, 10^{-6}]$ eV. Most existing axion detection proposals use some kind of resonant enhancement, but we have shown that broadband circuits can have superior sensitivity for lighter axion masses. This conclusion agrees with previous literature establishing that untuned SQUID magnetometers outperform tuned magnetometers at low frequencies [42,43]; this fact has been exploited in, e.g., Refs. [52,53] to detect fT magnetic fields from MRI experiments with biological tissue samples. A concrete experiment would likely proceed in two stages: a broadband search over a large frequency range, followed by a resonant scan at high frequencies and in specific frequency bands if a signal is seen. We expect that a broadband magnetometer could also be relevant for detecting dark photon DM [24], and we look forward to further applications of broadband techniques to light DM detection.

*ykahn@princeton.edu
†bsafdi@mit.edu
‡jthaler@mit.edu

[1] J. Preskill, M. B. Wise, and F. Wilczek, Phys. Lett. B **120**, 127 (1983).

[2] L. F. Abbott and P. Sikivie, Phys. Lett. B **120**, 133 (1983).

[3] M. Dine and W. Fischler, Phys. Lett. B **120**, 137 (1983).

[4] R. D. Peccei and H. R. Quinn, Phys. Rev. Lett. **38**, 1440 (1977).

[5] R. D. Peccei and H. R. Quinn, Phys. Rev. D **16**, 1791 (1977).

[6] S. Weinberg, Phys. Rev. Lett. **40**, 223 (1978).

[7] F. Wilczek, Phys. Rev. Lett. **40**, 279 (1978).

[8] P. Svrcek and E. Witten, J. High Energy Phys. 06 (2006) 051.

[9] R. Essig et al., in Community Summer Study 2013: Snowmass on the Mississippi (CSS2013) Minneapolis, MN, USA, July 29–August 6, 2013 (2013), arXiv:1311.0029.

[10] D. J. E. Marsh, Phys. Rep. **643**, 1 (2016).

[11] P. W. Graham, I. G. Irastorza, S. K. Lamoreaux, A. Lindner, and K. A. van Bibber, Annu. Rev. Nucl. Part. Sci. **65**, 485 (2015).

[12] S. J. Asztalos et al. (ADMX Collaboration), Phys. Rev. D **64**, 092003 (2001).

[13] S. J. Asztalos et al., Phys. Rev. Lett. **104**, 041301 (2010).

[14] T. M. Shokair et al., Int. J. Mod. Phys. A **29**, 1443004 (2014).

[15] J. I. Read, J. Phys. G **41**, 063101 (2014).

[16] P. Sikivie, Phys. Rev. Lett. **51**, 1415 (1983); **52**, 695(E) (1984).

[17] M. Dine, W. Fischler, and M. Srednicki, Phys. Lett. B **104**, 199 (1981).

[18] A. R. Zhitnitsky, Yad. Fiz. **31**, 497 (1980) [Sov. J. Nucl. Phys. **31**, 260 (1980)].

[19] J. E. Kim, Phys. Rev. Lett. **43**, 103 (1979).

[20] M. A. Shifman, A. I. Vainshtein, and V. I. Zakharov, Nucl. Phys. **B166**, 493 (1980).

[21] K. Grohmann, H. Hahlbohm, H. Lübbig, and H. Ramin, Cryogenics **14**, 499 (1974).

[22] P. Sikivie, N. Sullivan, and D. B. Tanner, Phys. Rev. Lett. **112**, 131301 (2014).

[23] S. Thomas and B. Cabrera, Detecting string-scale QCD axion dark matter, Axions 2010: Proceedings of the International Conference, http://scitation.aip.org/content/aip/proceeding/aipcp/1274.

[24] S. Chaudhuri, P. W. Graham, K. Irwin, J. Mardon, S. Rajendran, and Y. Zhao, Phys. Rev. D **92**, 075012 (2015).

[25] D. Budker, P. W. Graham, M. Ledbetter, S. Rajendran, and A. O. Sushkov, Phys. Rev. X **4**, 021030 (2014).

[26] O. K. Baker, M. Betz, F. Caspers, J. Jaeckel, A. Lindner, A. Ringwald, Y. Semertzidis, P. Sikivie, and K. Zioutas, Phys. Rev. D **85**, 035018 (2012).

[27] P. W. Graham and S. Rajendran, Phys. Rev. D **84**, 055013 (2011).

[28] P. W. Graham and S. Rajendran, Phys. Rev. D **88**, 035023 (2013).

[29] D. Horns, J. Jaeckel, A. Lindner, A. Lobanov, J. Redondo, and A. Ringwald, J. Cosmol. Astropart. Phys. 04 (2013) 016.

[30] D. Horns, A. Lindner, A. Lobanov, and A. Ringwald, in 9th Patras Workshop on Axions, WIMPs & WISPs (PATRAS13) Mainz, Germany, June 24-28, 2013 (2013), arXiv:1309.4170.

[31] Y. V. Stadnik and V. V. Flambaum, Phys. Rev. D **89**, 043522 (2014).

[32] C. Beck, Phys. Rev. Lett. **111**, 231801 (2013).

[33] C. Beck, Phys. Dark Univ. **7–8**, 6 (2015).

[34] J. Hong, J. E. Kim, S. Nam, and Y. Semertzidis, arXiv:1403.1576.

[35] B. M. Roberts, Y. V. Stadnik, V. A. Dzuba, V. V. Flambaum, N. Leefer, and D. Budker, Phys. Rev. Lett. **113**, 081601 (2014).

[36] B. M. Roberts, Y. V. Stadnik, V. A. Dzuba, V. V. Flambaum, N. Leefer, and D. Budker, Phys. Rev. D **90**, 096005 (2014).

[37] Y. V. Stadnik and V. V. Flambaum, Phys. Rev. Lett. **114**, 161301 (2015).

[38] C. T. Hill, Phys. Rev. D **91**, 111702 (2015).

[39] C. T. Hill, Phys. Rev. D **93**, 025007 (2016).

[40] B. T. McAllister, S. R. Parker, and M. E. Tobar, Phys. Rev. Lett. **116**, 161804 (2016).

[41] J. K. Vogel et al., arXiv:1302.3273.

[42] W. Myers, D. Slichter, M. Hatridge, S. Busch, M. Mößle, R. McDermott, A. Trabesinger, and J. Clarke, J. Magn. Reson. **186**, 182 (2007).

[43] J. Clarke, C. D. Tesche, and R. Giffard, J. Low Temp. Phys. **37**, 405 (1979).

[44] D. Shoenberg, Superconductivity (Cambridge University Press, Cambridge, England, 1954).

[45] J. Zimmerman, J. Appl. Phys. **42**, 4483 (1971).

[46] D. Drung, R. Cantor, M. Peters, H. Scheer, and H. Koch, Appl. Phys. Lett. **57**, 406 (1990).

[47] See Supplemental Material at http://link.aps.org/supplemental/10.1103/PhysRevLett.117.141801 for details of the signal-to-noise calculations presented in the main Letter, along with additional experimental considerations.

[48] S. Anton, J. Birenbaum, S. O'Kelley, V. Bolkhovsky, D. Braje, G. Fitch, M. Neeley, G. Hilton, H.-M. Cho, K. Irwin et al., Phys. Rev. Lett. **110**, 147002 (2013).

[49] H. Seton, D. Bussell, J. Hutchison, and D. Lurie, IEEE Trans. Appl. Supercond. **5**, 3218 (1995).

[50] H. Seton, J. Hutchison, and D. Bussell, Magnetic Resonance Materials in Physics, Biology, and Medicine **8**, 116 (1999).

[51] M. Bonaldi, P. Falferi, M. Cerdonio, A. Vinante, R. Dolesi, and S. Vitale, Rev. Sci. Instrum. **70**, 1851 (1999).

[52] A. N. Matlachov, P. L. Volegov, M. A. Espy, J. S. George, and R. H. Kraus, J. Magn. Reson. **170**, 1 (2004).

[53] R. McDermott, S. Lee, B. Ten Haken, A. H. Trabesinger, A. Pines, and J. Clarke, Proc. Natl. Acad. Sci. U.S.A. **101**, 7857 (2004).